Article

Organic reaction mechanism classification using machine learning

https://doi.org/10.1038/s41586-022-05639-4

Received: 15 February 2022

Accepted: 8 December 2022

Published online: 25 January 2023

Check for updates

Jordi Burés[1]✉ & Igor Larrosa[1]✉

A mechanistic understanding of catalytic organic reactions is crucial for the design of new catalysts, modes of reactivity and the development of greener and more sustainable chemical processes[1–13]. Kinetic analysis lies at the core of mechanistic elucidation by facilitating direct testing of mechanistic hypotheses from experimental data. Traditionally, kinetic analysis has relied on the use of initial rates[14], logarithmic plots and, more recently, visual kinetic methods[15–18], in combination with mathematical rate law derivations. However, the derivation of rate laws and their interpretation require numerous mathematical approximations and, as a result, they are prone to human error and are limited to reaction networks with only a few steps operating under steady state. Here we show that a deep neural network model can be trained to analyse ordinary kinetic data and automatically elucidate the corresponding mechanism class, without any additional user input. The model identifies a wide variety of classes of mechanism with outstanding accuracy, including mechanisms out of steady state such as those involving catalyst activation and deactivation steps, and performs excellently even when the kinetic data contain substantial error or only a few time points. Our results demonstrate that artificial-intelligence-guided mechanism classification is a powerful new tool that can streamline and automate mechanistic elucidation. We are making this model freely available to the community and we anticipate that this work will lead to further advances in the development of fully automated organic reaction discovery and development.

Determining the exact sequence of the elementary steps involved in transforming substrates into products is essential in regard to rational improvement of synthetic methods, design of new catalysts and safely scale-up industrial processes (Fig. 1a–d)[1–4]. To elucidate the mechanism of a reaction, several kinetic profiles are collected and human experts must carry out kinetic analysis of the data. Although reaction-monitoring technology has improved markedly during past decades to the point at which kinetic data collection can be fully automated[19–22], the underlying theoretical framework for mechanism elucidation has not advanced at the same pace. The current pipeline for kinetic analysis involves three broad steps (Fig. 1e, top path): extraction of kinetic properties from experimental data, prediction of the kinetic properties of all plausible mechanisms and comparison of experimentally extracted properties with those predicted. The method most commonly used to extract kinetic properties, despite its numerous pitfalls[23], is the log–log plot of initial rates developed over a century ago[14]. Modern kinetic analyses, such as reaction progress kinetic analysis[15,16] and variable time normalization analysis[17,18], extract richer kinetic information using entire kinetic profiles rather than only a small section of them. However, they miss implicit kinetic information embedded in the kinetic profiles because they focus on specific reaction properties, mainly orders of reaction. Prediction of kinetic properties also requires that chemists fully master the intricate derivation and interpretation of steady-state rate laws. Although steady-state equations are a good approximation to the kinetic behaviour of many mechanisms, they fail to predict commonly found systems far from steady state, such as reactions with slow catalyst activation or irreversible catalyst deactivation[24]. In addition, even moderately complex reaction networks can lead to unmanageable rate law equations that are exceedingly difficult to interpret. Alternatively, kinetic modelling has been used to fit kinetic data and, although it is a powerful engineering tool for parametrization of chemical processes, its applicability to mechanism elucidation is limited due to the difficulties involved in discriminating between models with similar goodness of fit[25].

Inspired by recent dramatic advances in the application of artificial intelligence (AI) to long-standing scientific challenges[26–33], we envisioned that AI could transform the field of kinetic analysis. Herein we demonstrate that a deep learning model trained on simulated kinetic data is capable of correctly elucidating a wide variety of classes of mechanisms from temporal concentration profiles (Fig. 1e, bottom path). The machine learning model eliminates the need for rate law derivations and kinetic property extraction and prediction, thus streamlining kinetic analysis and greatly facilitating the elucidation of reaction mechanisms to all synthetic laboratories. The method increases the capacity to interrogate reaction profiles because of the holistic analysis of all kinetic data available, removes potential human error from the kinetic analysis process and expands the scope of the kinetics that can be analysed to include non-steady-state (including activation and deactivation processes) and reversible reactions. We envision that this

[1]Department of Chemistry, The University of Manchester, Manchester, UK. ✉e-mail: jordi.bures@manchester.ac.uk; igor.larrosa@manchester.ac.uk

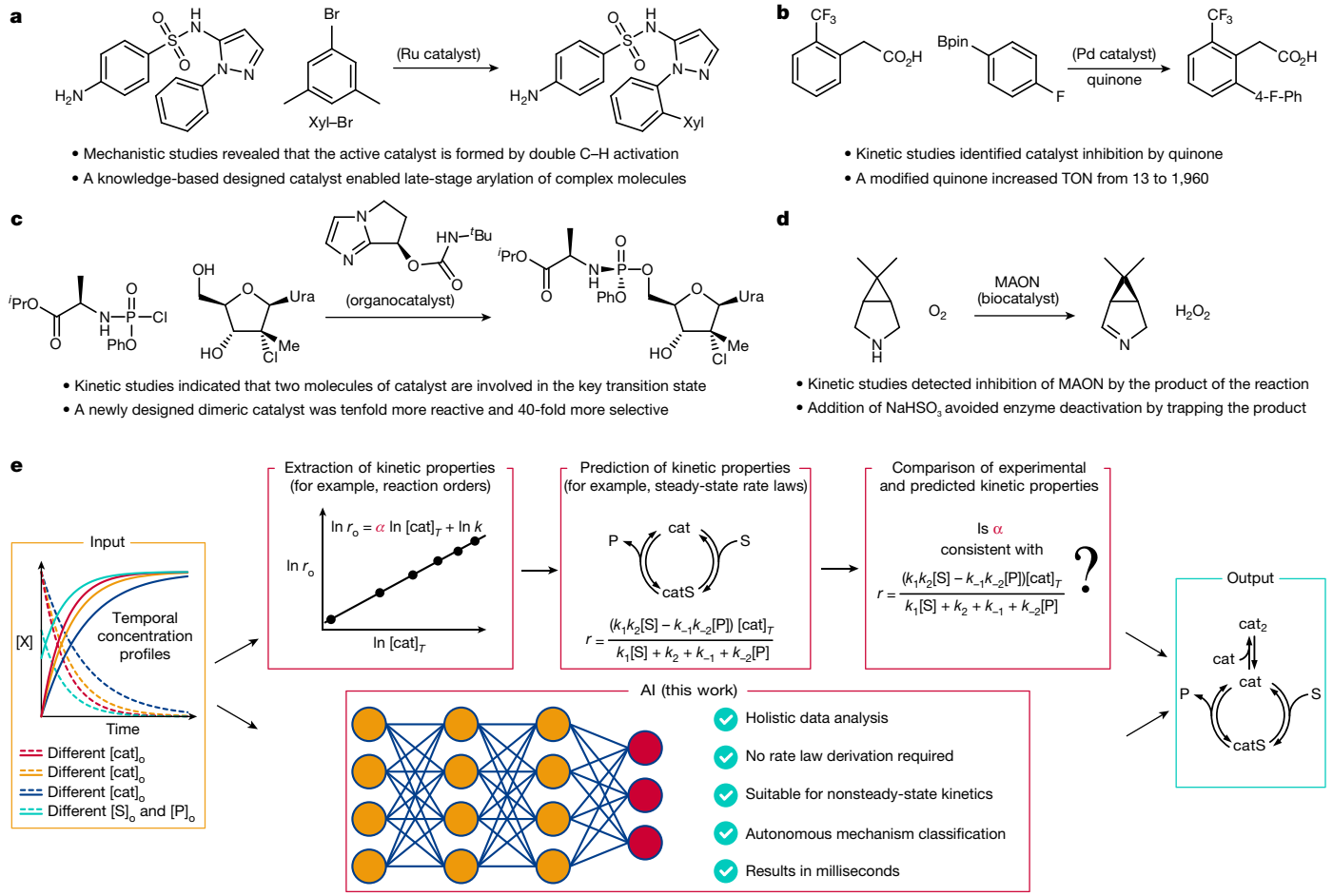

Fig. 1 | Relevance and state of the art on kinetic analysis. a, Mechanistic understanding of a Ru-catalysed arylation leads to a new catalyst with over 100-fold increase in reactivity. **b**, Mechanistic understanding of a Pd-catalysed arylation leads to 150-fold increase in catalyst turnover number (TON). **c**, Mechanistic knowledge of an industrially relevant organocatalytic reaction enabled the design of a catalyst tenfold more reactive and 40-fold more selective. **d**, Kinetic investigations facilitated the development of an efficient process with low amounts of monoamine oxidase from *Aspergillus niger* (MAON). **e**, Comparison of current pipeline for mechanistic elucidation through kinetic analysis versus the use of our new, AI-based mechanistic elucidation.

method will be complementary to currently available kinetic analysis methods and will be especially useful in the most challenging cases.

We considered 20 commonly encountered mechanisms of reactions converting substrate (S) to product (P) mediated by a catalyst (cat) (Fig. 2a). These mechanisms belong to four distinct categories (Fig. 2a): (1) the core mechanism (M1), which is the simplest Michaelis–Menten-type mechanism[14]; (2) mechanisms with bicatalytic steps (M2–M5) that involve either catalyst dimerization (M2 and M3) or a reaction between two different catalytic species (M4 and M5); (3) mechanisms with catalyst activation steps based on the core mechanism, in which a precatalyst requires activation unimolecularly (M6) via either substrate coordination (M7) or ligand dissociation (M8); and (4) mechanisms with a variety of catalyst deactivation steps from either catalytic intermediate of the core mechanism (M9–M20), which are often extremely challenging to differentiate but are encountered in the vast majority of catalytic processes.

Each mechanism is mathematically described by a set of ordinary differential equations (ODEs) function of kinetic constants (k_1, … k_n) and concentration of chemical species (Supplementary Information). These equations allow the generation of an infinite number of temporal concentration profiles of substrate and products, defining a kinetic space. Although kinetic spaces are characteristic for each mechanism, they can partially overlap. For example, if a particular set of kinetic constants for M2 results in no substantial formation of the off-cycle dimer cat_2, the resulting kinetic profiles are indistinguishable from those of the core mechanism, M1 (Fig. 2b). Overlaps between classes—in our case, mechanisms—are well known to have detrimental effects on the performance of learning algorithms[34,35]. To minimize these overlaps we used chemical criteria (Supplementary Information) to define the kinetic space of each mechanism, giving preference to the simplest mechanisms and therefore avoiding the classification of kinetic concentration profiles to overcomplicated mechanisms with insufficient kinetic evidence.

The training of deep learning models typically requires large amounts of data, which can pose a considerable challenge when these data must be collected experimentally. However, in our case we were able to generate 5 million kinetic samples for the training and validation of the model by numerically solving the sets of ODEs, without having to use steady-state approximation. Each kinetic sample, used as input of the deep neural network, contains four temporal concentration profiles from a particular mechanism with a fixed set of kinetic constant values; three of the profiles have identical initial concentration of substrate ($[S]_0$) but different $[cat]_0$ in the range 1–10 mol%, and the fourth is a 'same-excess' experiment[15] with reduced $[S]_0$ (Fig. 2c) and product added ($[P]_0$). We chose this combination of experiments because it includes the necessary information to differentiate between the set of potential mechanisms considered (Fig. 2a). Specifically, experiments with different concentrations of catalyst help in the assessment of the presence of mechanistic steps involving more than one catalytic species, and same-excess experiments

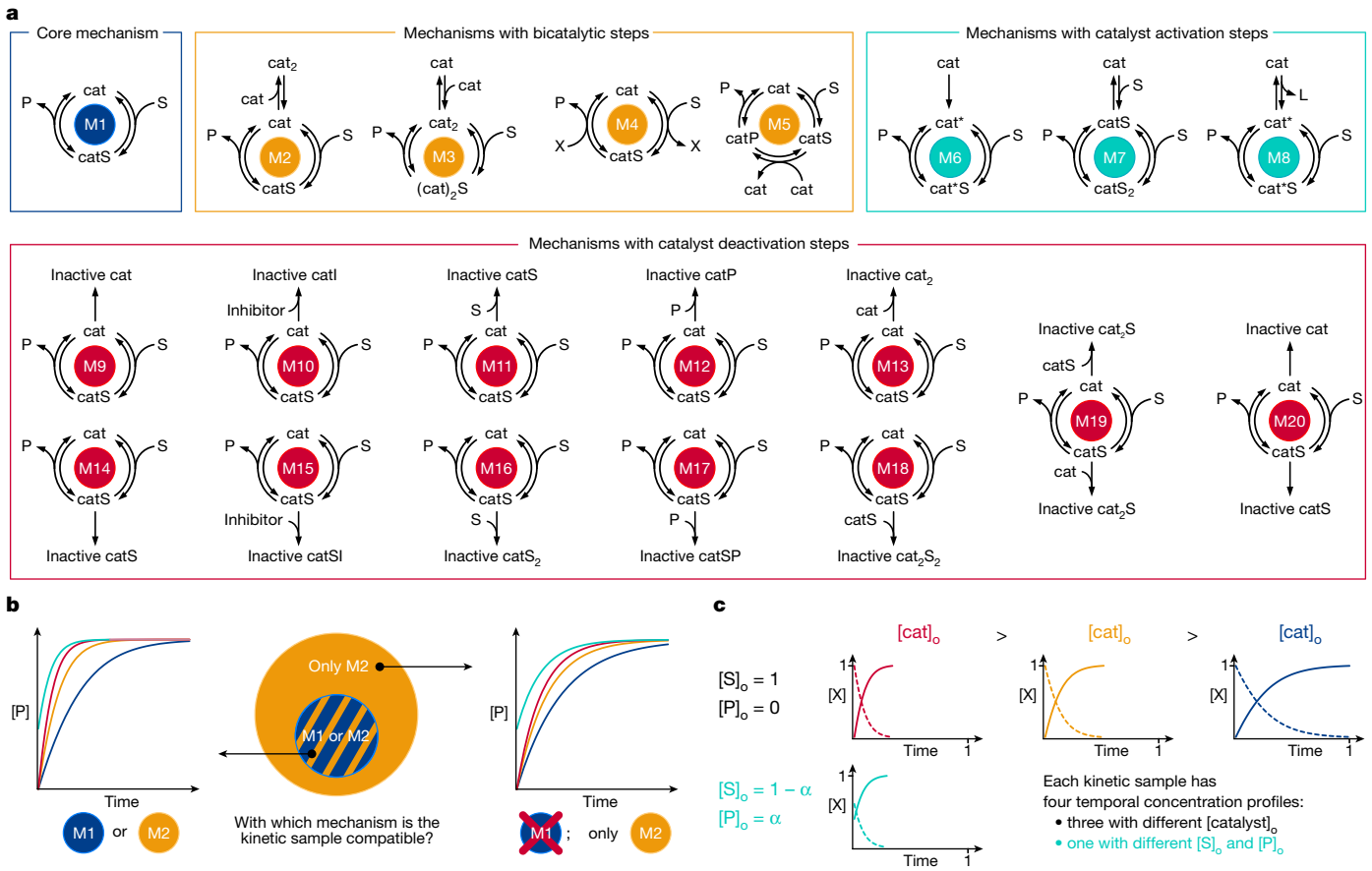

Fig. 2 | Mechanism scope and composition of data. a, Twenty mechanisms under consideration, grouped in four basic categories. cat*, activated catalyst. **b**, The kinetic space of some mechanisms overlaps partially. **c**, Composition of a kinetic sample for training, validation or testing. [X] refers to the concentration of S or P.

provide information about both product inhibition and the activation and deactivation processes of the catalyst. The profiles include concentration of substrate and product at 20 randomly selected times, which ensures a breadth of profiles with data heterogeneously distributed over time and covering different ranges of conversions (see Supplementary Information for a detailed description of the data generation process).

Our model contains 576,000 trainable parameters and uses a combination of two types of neural network: (1) long short-term memory neural networks, a type of recurrent neural network used to process sequences of temporal data (that is, the temporal concentration data) and (2) fully connected neural networks, used to process atemporal data (that is, the initial concentrations of catalyst in each kinetic run and features extracted by the long short-term memory). The model outputs probabilities for each mechanism, with the total sum of probabilities equalling 1 (for a full description of the model architecture see Supplementary Information). Data augmentation was applied during training, which involved (1) reducing the number of concentration–time points in the sample from 20 to any value in the range 20–3 and (2) introducing Gaussian error on the sample concentration values of S and P, with a s.d. up to 2%. Evaluation of the model with the validation set during training showed little to no overfitting, probably due to the varied and large training set (Supplementary Fig. 4).

The trained model was evaluated with a test set of 100,000 kinetic samples (5,000 per mechanism) containing six concentration–time points per profile, a typical number of data points collected when sampling reactions. Importantly, all kinetic samples in the test set belong to unique kinetic profiles, different to those used in the training set (Supplementary Information). The model afforded a categorical accuracy of 92.6%, confusion entropy[36] of 0.053 and top-three accuracy of 100% with this test set. Other machine learning methods, such as similarity search, support vector machines and random forest, provided much inferior results (Supplementary Information). Interestingly, analysis of the confusion matrix plotting the actual mechanism against the predicted mechanism (Fig. 3a) showed that most mechanisms are correctly predicted with very high recall, with most mistakes clustering between two activation mechanisms (M6 and M8) and between three deactivation mechanisms (M11, M12 and M14). Analysis of the probability curves predicted for the samples of each mechanism (Fig. 3b) shows that, in the majority of test samples, the model not only predicts the correct mechanism but also does so with very high confidence (over 99%). Test samples with lower confidence are mostly due to overlap of kinetic spaces. For example, a large section of the sample pools of M11 and M14 has a confidence of around 50% because both mechanisms can have kinetic profiles in which catalyst deactivation depends identically on substrate concentration and, therefore, some of their profiles are indistinguishable. Because we consider both mechanisms to have similar complexity, we decided not to assign the common kinetic space exclusively to one of them, which would have resulted in an artificial hierarchy between them. On the contrary, we welcomed these crosses between mechanistic predictions because they demonstrate that the model is capable not only of correct classification of most mechanisms, but also of identification of sets of data that are consistent with more than one mechanism and assigning them a substantial probability. Taking advantage of this quality of the model, we decided to generate more flexible and valuable outcomes by grouping the top predictions until achieving a cumulative confidence threshold higher than 99%. By allowing the grouping of predicted mechanisms (Fig. 3c), model categorical accuracy increased to 99.96% (a total of only 38 mistakes in the 100,000 sample test set), with 69,740 samples of the test set predicted as unique mechanisms, 23,767 with two proposed mechanisms, 6,067 with three and a residual

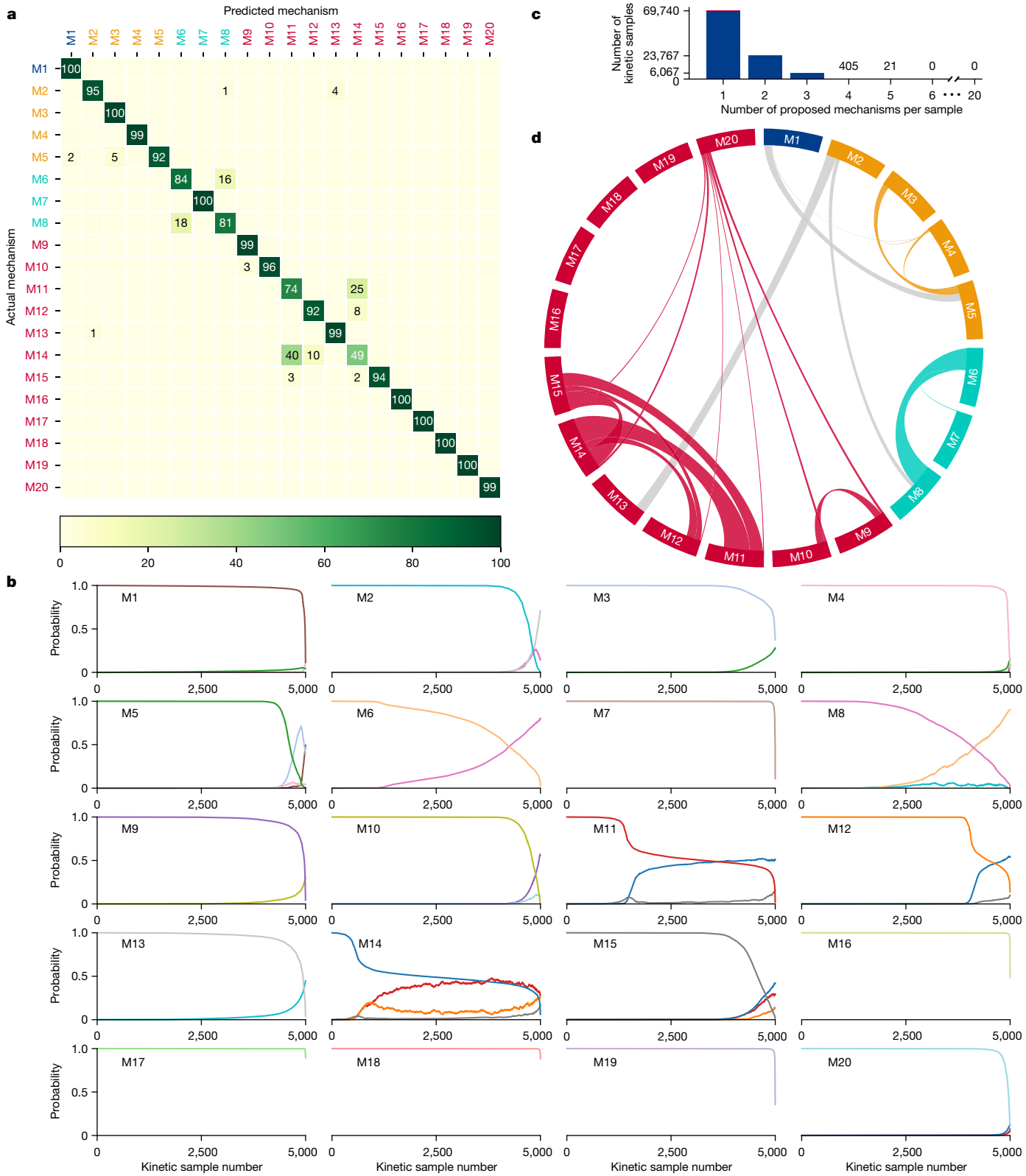

Fig. 3 | Performance of the machine learning model on the test set with six time points per kinetic profile. a, Top predicted mechanism versus actual mechanism (in percentage). **b**, Predicted probabilities for the 5,000 true test kinetic samples of each mechanism (200 sample moving average), ordered from highest to lowest probability for the corresponding mechanism. For clarity, only curves containing at least one predicted value above 0.1 are shown. **c**, Number of mechanisms predicted together by the model with 99% confidence threshold. **d**, Circos plot showing mechanisms grouped in the model's predictions with 99% confidence threshold. The thickness of each ribbon linking two mechanisms is proportional to the number of times these mechanisms are grouped.

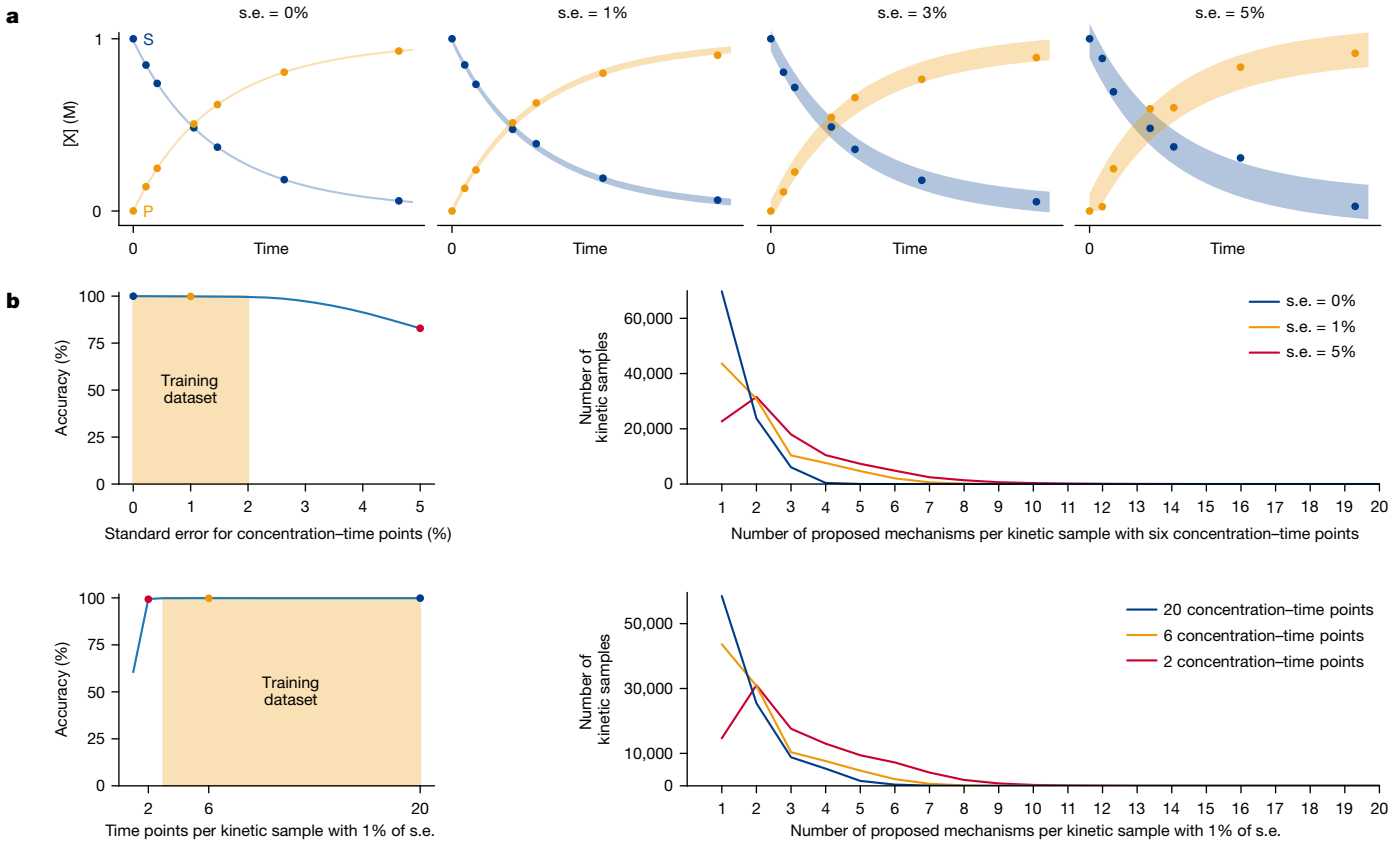

Fig. 4 | Effect of error and amount of data points in the performance of the machine learning model. a, Example of kinetic data for different levels of Gaussian error, with shading representing confidence interval 95%. **b**, Accuracy (left) and grouping of mechanisms (right) at different s.d. in concentration–time points (top) and number of points per kinetic sample (bottom).

0.43% with more than three (for further analysis see Supplementary Information). Remarkably the model tends to group mechanisms within the same category, with very few crossings between categories (Fig. 3d). This result suggests that most of the original 7.4% inaccuracy obtained with single mechanistic classifications was due to overlaps between mechanisms that should, indeed, be proposed together.

To fully explore the potential of our machine learning model, we investigated the effect of introducing error in the data and changing the number of data points provided. Temporal concentration profiles with Gaussian s.d. up to 2% (plus or minus 4% on yield with 95% confidence interval) in concentration (Fig. 4a) are commonly found experimentally[37]. Extraction of information from profiles with so much error is one of the biggest challenges in kinetic analyses[38–40] and therefore is an excellent test for our model. We introduced various levels of Gaussian error (up to 5% s.d.) on the concentration variable of the original test set. Remarkably, when the resulting test sets were evaluated, the model was able to maintain very high categorical accuracy (over 99.6%) even with appreciable standard error (s.e., up to 2%) in the data (Fig. 4b, top left). Even for poor-quality data (that is, s.e. = 5% or an error of plus or minus 10% in yield with 95% confidence interval), a categorical accuracy of 83% was achieved. The model copes with the inherent uncertainty introduced by the error in the data by increasing the number of mechanisms grouped in its predictions (Fig. 4b, top right). Circos plots of the mechanisms grouped for test sample data containing 1% and 5% s.d. (Supplementary Figs. 8 and 9) show that whereas grouping is maintained within the same mechanistic category for the dataset with s.e. = 1%, crossings between categories of mechanisms appear with s.e. = 5%. The latter is not unexpected because the distortion of kinetic profiles is very large and therefore the resulting sample data could truly belong to mechanisms from different categories. The model responds similarly to the presence of outliers (Supplementary Information) but these results are less relevant because, experimentally, one would normally exclude obvious outliers from analysis using any kinetic analytical techniques.

A common strategy used to mitigate the inaccuracy derived from error in the data is to increase the amount of data. We explored the effect of varying the number of concentration–time points provided to the model for its predictions using a dataset with 1% s.e. (Fig. 4b, bottom left). High categorical accuracy was obtained across the board for test sets containing between two and 20 concentration–time points. The model is able to use the additional time point information to increase the proportion of predictions in which a single mechanism is correctly proposed (Fig. 4b, bottom right). Conversely, the number of grouped mechanisms increases when concentration–time points are decreased below six. Despite the model never having been trained with samples containing fewer than three concentration–time points, it still performs remarkably well with a test set containing only two data points per kinetic profile.

To exemplify the potential of AI models in analysis of experimental kinetic data, we applied it to a diverse range of catalytic reactions including ring-closing olefin metathesis[41], cycloadditions[42], alkene isomerizations[43], C–H aminations[44], photocatalysed hydroalcoxylations[45] and carbonyl–olefin metathesis[46,47] (Fig. 5). These case studies include examples in which the kinetic data contain only three reaction profiles at varying catalyst concentration (that is, without the same-excess experiment), as well as examples in which only substrate or product is monitored. In all cases the machine learning models have been able to identify the important characteristic mechanistic features of each system, matching those proposed by the authors through kinetic and additional mechanistic experiments. More remarkably, the models have also proposed mechanisms that could not be demonstrated by traditional kinetic analyses, such as specific catalyst deactivation

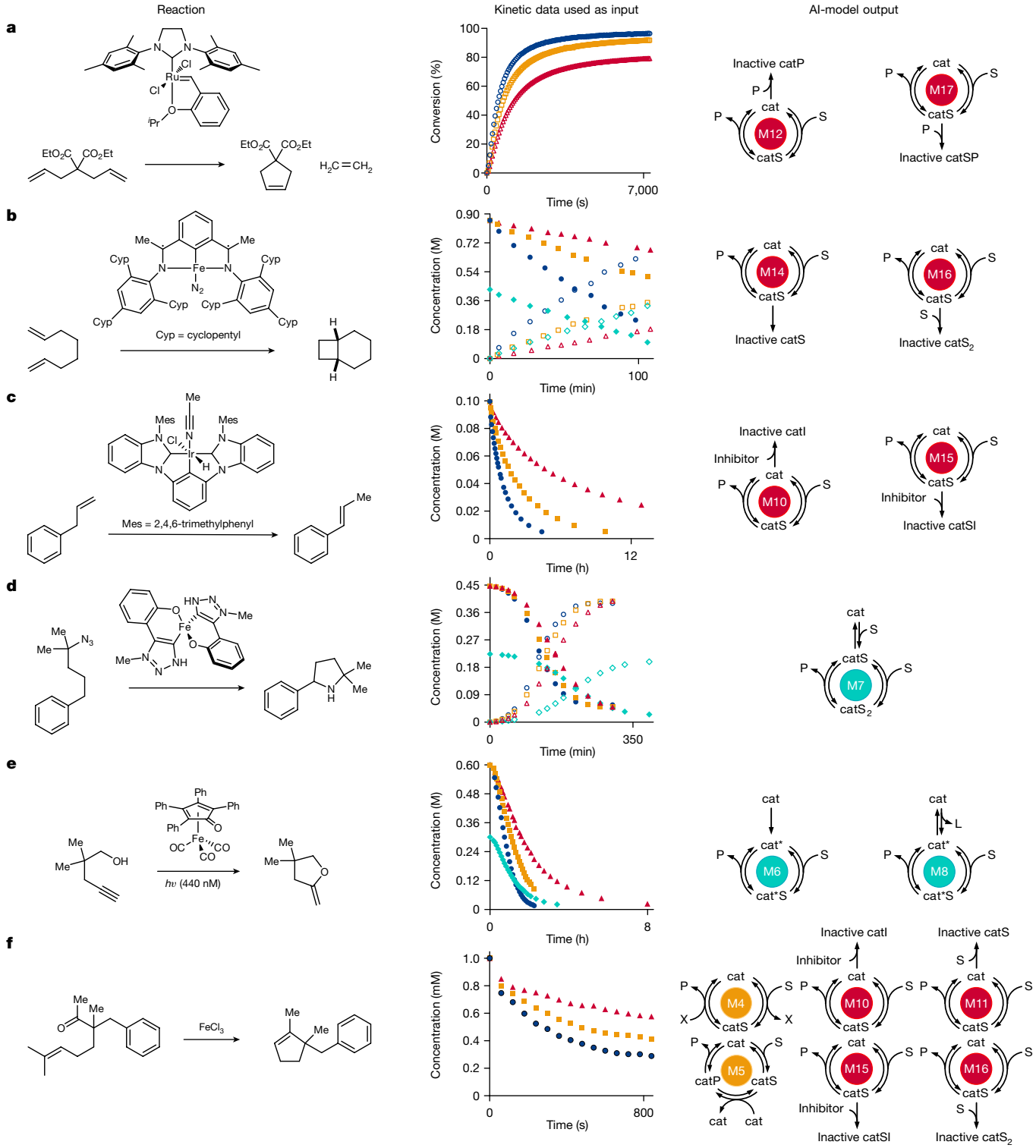

Fig. 5 | Case studies with experimental kinetic data. Each row includes the reaction under study, the experimental kinetic data used as input for the AI model and output. Filled symbols, substrate concentration; hollow symbols, product concentration; red triangles, lowest catalyst loading; yellow squares, medium catalyst loading; blue circles, largest catalyst loading; turquoise diamonds, lower concentration of substrate. **a**, A ring-closing metathesis with proposed catalyst deactivation by product. **b**, A [2+2]-cycloaddition reaction with proposed catalyst deactivation by substrate. **c**, An alkene isomerization with proposed catalyst deactivation by an inhibitor. **d**, A C–H amination with proposed catalyst activation by substrate. **e**, An alkyne hydroalkoxylation with proposed catalyst activation by ligand dissociation. **f**, A carbonyl-olefin metathesis with either catalyst deactivation or bicatalytic steps. Data from ref. [41] (**a**), ref. [42] (**b**), ref. [43] (**c**), ref. [44] (**d**), ref. [45] (**e**), ref. [47] (**f**).

pathways. In the case of the ring-closing olefin metathesis reported by Thiel et al.[41] (Fig. 5a), the machine learning model is able not only to recognize the catalyst deactivation proposed by the authors but also to implicate the product on the deactivation pathway. The prediction of the model is in agreement with previous work carried out on stoichiometric Ru complexes and density functional theory calculations[48,49],

which indeed showed the possibility of the ethene product inducing catalyst decomposition. Similarly, in the [2 + 2] cycloaddition reaction reported by Joannou et al.[42] (Fig. 5b), the machine learning model identifies deactivation of the catalyst with involvement of the substrate of the reaction. Although classic kinetic analysis had not allowed identification of this mechanistic feature because of its subtle effect on kinetic data[42], the authors had observed in stoichiometric organometallic studies a substrate-mediated dehydrogenative deactivation of the catalyst. Another deactivation process not immediately obvious was shown by the machine learning model in the alkene isomerization reported by Knapp et al.[43] (Fig. 5c). The AI models also identify highly specific catalyst activation processes, as in the case of the C–H amination reported by Stroek et al.[44] (Fig. 5d) and the hydroalcoxylation by Lehnherr et al.[45] (Fig. 5e). In the case of the carbonyl–olefin metathesis reported by Ludwig et al.[46] and Albright et al.[47] (Extended Data Fig. 1 and Fig. 5f), the model proposes the largest number of mechanistic possibilities among the seven case studies, which suggests that extra experiments would be desirable to increase accuracy in this case. This especially challenging case shows the potential for AI-guided design of new kinetic experiments and refinement of mechanistic proposals.

In conclusion, we have demonstrated that deep learning can be leveraged to provide an extremely powerful tool for mechanistic elucidation from kinetic data. The new model simplifies the previous lengthy process of rate law derivation and kinetic analysis into an integrated and more accurate process that requires merely milliseconds. The trained model is able to resolve complex problems for which analysis was previously very challenging, such as kinetic data with error and even systems out of steady state. We have also shown how these AI models can be readily applied to extract mechanistic insights using experimental kinetic data from a variety of catalytic reactions. We envision that machine learning will become a powerful tool, enhancing the ability of synthetic chemists to tackle mechanistic investigations.

Online content

Any methods, additional references, Nature Portfolio reporting summaries, source data, extended data, supplementary information, acknowledgements, peer review information; details of author contributions and competing interests; and statements of data and code availability are available at https://doi.org/10.1038/s41586-022-05639-4.

1. Simonetti, M., Cannas, D. M., Just-Baringo, X., Vitorica-Yrezabal, I. J. & Larrosa, I. Cyclometallated ruthenium catalyst enables late-stage directed arylation of pharmaceuticals. *Nat. Chem.* **10**, 724–731 (2018).
2. Salazar, C. A. et al. Tailored quinones support high-turnover Pd catalysts for oxidative C-H arylation with O_2. *Science* **370**, 1454–1460 (2020).
3. DiRocco, D. A. et al. A multifunctional catalyst that stereoselectively assembles prodrugs. *Science* **356**, 426–430 (2017).
4. Li, T. et al. Efficient, chemoenzymatic process for manufacture of the Boceprevir bicyclic [3.1.0]proline intermediate based on amine oxidase-catalyzed desymmetrization. *J. Am. Chem. Soc.* **134**, 6467–6472 (2012).
5. Nielsen, L. P., Stevenson, C. P., Blackmond, D. G. & Jacobsen, E. N. Mechanistic investigation leads to a synthetic improvement in the hydrolytic kinetic resolution of terminal epoxides. *J. Am. Chem. Soc.* **126**, 1360–1362 (2004).
6. van Dijk, L. et al. Mechanistic investigation of Rh(I)-catalysed asymmetric Suzuki–Miyaura coupling with racemic allyl halides. *Nat. Catal.* **4**, 284–292 (2021).
7. Camasso, N. M. & Sanford, M. S. Design, synthesis, and carbon-heteroatom coupling reactions of organometallic nickel(IV) complexes. *Science* **347**, 1218–1220 (2015).
8. Milo, A., Neel, A. J., Toste, F. D. & Sigman, M. S. A data-intensive approach to mechanistic elucidation applied to chiral anion catalysis. *Science* **347**, 737–743 (2015).
9. Butcher, T. W. et al. Desymmetrization of difluoromethylene groups by C-F bond activation. *Nature* **583**, 548–553 (2020).
10. Cho, E. J. et al. The palladium-catalyzed trifluoromethylation of aryl chlorides. *Science* **328**, 1679–1681 (2010).
11. Hutchinson, G., Alamillo-Ferrer, C. & Bures, J. Mechanistically guided design of an efficient and enantioselective aminocatalytic alpha-chlorination of aldehydes. *J. Am. Chem. Soc.* **143**, 6805–6809 (2021).
12. Schreyer, L. et al. Confined acids catalyze asymmetric single aldolizations of acetaldehyde enolates. *Science* **362**, 216–219 (2018).
13. Peters, B. K. et al. Scalable and safe synthetic organic electroreduction inspired by Li-ion battery chemistry. *Science* **363**, 838–845 (2019).
14. Michaelis, L. & Menten, M. L. Die Kinetik der Invertinwirkung. *Biochem. Z.* **49**, 333–369 (1913).
15. Blackmond, D. G. Reaction progress kinetic analysis: a powerful methodology for mechanistic studies of complex catalytic reactions. *Angew. Chem. Int. Ed. Engl.* **44**, 4302–4320 (2005).
16. Mathew, J. S. et al. Investigations of Pd-catalyzed ArX coupling reactions informed by reaction progress kinetic analysis. *J. Org. Chem.* **71**, 4711–4722 (2006).
17. Bures, J. A simple graphical method to determine the order in catalyst. *Angew. Chem. Int. Ed. Engl.* **55**, 2028–2031 (2016).
18. Burés, J. Variable time normalization analysis: general graphical elucidation of reaction orders from concentration profiles. *Angew. Chem. Int. Ed. Engl.* **55**, 16084–16087 (2016).
19. Shi, Y., Prieto, P. L., Zepel, T., Grunert, S. & Hein, J. E. Automated experimentation powers data science in chemistry. *Acc. Chem. Res.* **54**, 546–555 (2021).
20. Burger, B. et al. A mobile robotic chemist. *Nature* **583**, 237–241 (2020).
21. Bedard, A. C. et al. Reconfigurable system for automated optimization of diverse chemical reactions. *Science* **361**, 1220–1225 (2018).
22. Steiner, S. et al. Organic synthesis in a modular robotic system driven by a chemical programming language. *Science* **363**, eaav2211 (2019).
23. Clauset, A., Shalizi, C. R. & Newman, M. E. J. Power-law distributions in empirical data. *SIAM Rev.* **51**, 661–703 (2009).
24. Martinez-Carrion, A. et al. Kinetic treatments for catalyst activation and deactivation processes based on variable time normalization analysis. *Angew. Chem. Int. Ed. Engl.* **58**, 10189–10193 (2019).
25. Bernacki, J. P. & Murphy, R. M. Model discrimination and mechanistic interpretation of kinetic data in protein aggregation studies. *Biophys. J.* **96**, 2871–2887 (2009).
26. Pfluger, P. M. & Glorius, F. Molecular machine learning: the future of synthetic chemistry? *Angew. Chem. Int. Ed. Engl.* **59**, 18860–18865 (2020).
27. Segler, M. H. S., Preuss, M. & Waller, M. P. Planning chemical syntheses with deep neural networks and symbolic AI. *Nature* **555**, 604–610 (2018).
28. Raissi, M., Yazdani, A. & Karniadakis, G. E. Hidden fluid mechanics: learning velocity and pressure fields from flow visualizations. *Science* **367**, 1026–1030 (2020).
29. Hermann, J., Schatzle, Z. & Noe, F. Deep-neural-network solution of the electronic Schrodinger equation. *Nat. Chem.* **12**, 891–897 (2020).
30. Shields, B. J. et al. Bayesian reaction optimization as a tool for chemical synthesis. *Nature* **590**, 89–96 (2021).
31. Tunyasuvunakool, K. et al. Highly accurate protein structure prediction for the human proteome. *Nature* **596**, 590–596 (2021).
32. Jumper, J. et al. Highly accurate protein structure prediction with AlphaFold. *Nature* **596**, 583–589 (2021).
33. Hueffel, J. A. et al. Accelerated dinuclear palladium catalyst identification through unsupervised machine learning. *Science* **374**, 1134–1140 (2021).
34. Haitao, X., Junjie, W. & Lu, L. In *Proc. 1st International Conference on E-Business Intelligence* 303–309 (Atlantis Press, 2010).
35. Batista, G. E. A. P. A. et al. In *Advances in Intelligent Data Analysis VI* (eds Fazel Famili, A. et al.) 24–35 (Springer, 2005).
36. Wei, J.-M., Yuan, X.-J., Hu, Q.-H. & Wang, S.-Q. A novel measure for evaluating classifiers. *Expert Syst. Appl.* **37**, 3799–3809 (2010).
37. Alberton, A. L., Schwaab, M., Schmal, M. & Pinto, J. C. Experimental errors in kinetic tests and its influence on the precision of estimated parameters. Part I—analysis of first-order reactions. *Chem. Eng. J.* **155**, 816–823 (2009).
38. Pacheco, H., Thiengo, F., Schmal, M. & Pinto, J. C. A family of kinetic distributions for interpretation of experimental fluctuations in kinetic problems. *Chem. Eng. J.* **332**, 303–311 (2018).
39. Storer, A. C., Darlison, M. G. & Cornish-Bowden, A. The nature of experimental error in enzyme kinetic measurments. *Biochem. J* **151**, 361–367 (1975).
40. Valkó, É. & Turányi, T. In Lindner, E., Micheletti, A. & Nunes, C. (eds) *Mathematical Modelling in Real Life Problems. Mathematics in Industry* https://doi.org/10.1007/978-3-030-50388-8_3 (2020).
41. Thiel, V., Wannowius, K. J., Wolff, C., Thiele, C. M. & Plenio, H. Ring-closing metathesis reactions: interpretation of conversion-time data. *Chem. Eur. J.* **19**, 16403–16414 (2013).
42. Joannou, M. V., Hoyt, J. M. & Chirik, P. J. Investigations into the mechanism of inter- and intramolecular iron-catalyzed [2 + 2] cycloaddition of alkenes. *J. Am. Chem. Soc.* **142**, 5314–5330 (2020).
43. Knapp, S. M. M. et al. Mechanistic studies of alkene isomerization catalyzed by CCC-pincer complexes of iridium. *Organometallics* **33**, 473–484 (2014).
44. Stroek, W., Keilwerth, M., Pividori, D. M., Meyer, K. & Albrecht, M. An iron-mesoionic carbene complex for catalytic intramolecular C-H amination utilizing organic azides. *J. Am. Chem. Soc.* **143**, 20157–20165 (2021).
45. Lehnherr, D. et al. Discovery of a photoinduced dark catalytic cycle using in situ LED-NMR spectroscopy. *J. Am. Chem. Soc.* **140**, 13843–13853 (2018).
46. Ludwig, J. R., Zimmerman, P. M., Gianino, J. B. & Schindler, C. S. Iron(III)-catalysed carbonyl-olefin metathesis. *Nature* **533**, 374–379 (2016).
47. Albright, H. et al. Catalytic carbonyl-olefin metathesis of aliphatic ketones: iron(III) homodimers as Lewis acidic superelectrophiles. *J. Am. Chem. Soc.* **141**, 1690–1700 (2019).
48. Janse van Rensburg, W., Steynberg, P. J., Meyer, W. H., Kirk, M. M. & Forman, G. S. DFT prediction and experimental observation of substrate-induced catalyst decomposition in ruthenium-catalyzed olefin metathesis. *J. Am. Chem. Soc.* **126**, 14332–14333 (2004).
49. van der Eide, E. F. & Piers, W. E. Mechanistic insights into the ruthenium-catalysed diene ring-closing metathesis reaction. *Nat. Chem.* **2**, 571–576 (2010).

Data availability

The datasets generated for training, validation and testing are available from figshare: https://doi.org/10.48420/16965292.

Code availability

Trained models, weights and python scripts are available from https://doi.org/10.48420/16965271.

Acknowledgements We thank the European Research Council for an Advanced Grant (no. 833337 to I.L.) and Research IT for assistance given and use of the Computational Shared Facility at The University of Manchester. We thank H. Plenio, P. J. Chirick, A. R. Chianese, M. Albrecht and C. S. Schindler for providing the numerical experimental kinetic data used in this study.

Author contributions I.L. and J.B. conceived the project. J.B. selected the mechanisms with input from I.L. I.L. wrote the code, created the datasets and trained the models with input from J.B. I.L. and J.B. analysed data. I.L. and J.B. wrote the manuscript.

Competing interests The authors declare no competing interests.

Additional information

Supplementary information The online version contains supplementary material available at https://doi.org/10.1038/s41586-022-05639-4.

Correspondence and requests for materials should be addressed to Jordi Burés or Igor Larrosa.

Peer review information *Nature* thanks Tiago Rodrigues and the other, anonymous, reviewer(s) for their contribution to the peer review of this work.

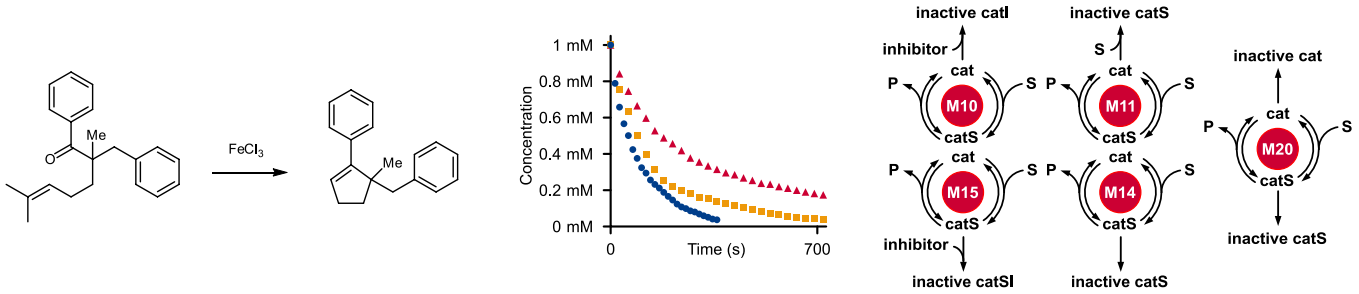

Extended Data Fig. 1 | Additional case study with experimental kinetic data. Includes the reaction under study, the experimental kinetic data used as input for the AI-model and its output. Symbols correspond to substrate concentration. Red triangles: lowest catalyst loading; yellow squares: medium catalyst loading; blue circles: largest catalyst loading. Data from ref. [47].